Chemical Engineering Science 63 (2008) 4386 – 4395

Contents lists available at ScienceDirect

Chemical Engineering Science

journal homepage: www.elsevier.com/locate/ces

Design and optimization of heat exchangers with helical baffles

Yong-Gang Lei, Ya-Ling He*, Pan Chu, Rui Li

State Key Laboratory of Multiphase Flow in Power Engineering, School of Energy and Power Engineering, Xi'an Jiaotong University, Xi'an, Shaanxi 710049, China

ARTICLE INFO

Article history:
Received 26 December 2007
Received in revised form 28 April 2008
Accepted 22 May 2008
Available online 4 June 2008

Keywords:
Helical baffles
Heat transfer
Pressure drop
Computational fluid dynamics (CFD)
Optimization

ABSTRACT

The hydrodynamics and heat transfer characteristics of a heat exchanger with single-helical baffles are studied experimentally as well as numerically. A heat exchanger with two-layer helical baffles is designed by using computational fluid dynamics (CFD) method. The comparisons of the performance of three heat exchangers with single-segment baffles, single-helical baffles and two-layer helical baffles, respectively, are presented in the paper. The experiment is carried out in counter-current flow pattern with hot oil in shell side and cold water in tube side. Overall heat transfer coefficients are calculated and heat transfer coefficients of shell side are determined by Wilson plots technique. It shows that the heat exchangers with helical baffles have higher heat transfer coefficient to the same pressure drop than that of the heat exchanger with segmental baffles based on the present numerical results, and the configuration of the two-layer helical baffles has better integrated performance than that of the single-helical baffles.

1. Introduction

Shell-and-tube heat exchangers are widely used in chemical, power generation, and petroleum refining industries. The baffles are of primary importance in heat exchangers because they force the shell-side fluid to flow across the tubes to ensure high heat transfer rates and provide support to tube bundles. The most commonly used baffle, the segmental baffle, improves heat transfer by enhancing turbulence or local mixing on the shell side of heat exchangers, but at the cost of a high pressure drop (Webb, 1994; Sthlik and Wadekar, 2002; Soltan et al., 2004). Various types of baffles such as deflector baffles, disk-and-donut configuration have been used in shell-and-tube heat exchangers to improve heat transfer while maintaining a reasonable pressure drop across the heat exchangers, but the principal shortcomings of conventional baffle design still remain (Mukherjee, 1992; Saffar-Avval and Damangir, 1995; Li and Kottke, 1998; Bell, 2004). Recently, a new type of heat exchanger with helical baffles is proposed to improve the performance on the shell side (Lutcha and Nemcansky, 1990; Stehlik et al., 1994; Kral et al., 1996). The helical baffles eliminate the pressure losses caused by change of flow direction and maintain helical flow on the shell side, thus resulting in the improvement of heat transfer and pressure drop characteristics.

Heat exchangers with helical baffles in shell side have higher ratio of heat transfer coefficient to pressure drop than that of heat exchanger with segmental baffles. Some experimental investigations of this type of heat exchanger have been conducted. Lutcha and Nemcansky (1990) investigated the flow pattern and heat transfer of tubular heat exchangers with helical baffles. They found that properly arranged helical baffles in tubular heat exchanger could force the shell side flow field to approach a plug flow condition, which increased the average temperature driving force due to the reduction of back mixing. The velocity gradient within the helical channel induced by the baffles also increased the shell side heat transfer markedly. Stehlik et al. (1994) compared heat transfer and pressure drop correction factors for an optimized segmental baffle heat exchanger with those for a helical baffle heat exchanger. In their studies, the correction factors for helical baffles were examined as a function of baffle inclination angle to better understand the underlying transport phenomena as well as to characterize the baffle for design purpose. Kral et al. (1996) discussed the performance of heat exchangers with helical baffles based on test results of various baffles geometries. Wang (2002) measured the flow field in shell-and-tube heat exchangers with helical baffles using laser Doppler anemometry. He pointed out that the optimum helix inclination angle depends on the Reynolds number of the working fluid on the shell side of the heat exchanger. Zhang et al. (2004) presented an experimental investigation of heat transfer and pressure drop of a helically baffled heat exchanger with petal-shaped finned tubes.

A comprehensive experimental investigation of a heat exchanger is very expensive because of the high equipment cost. In comparison with experimental study, a validated computational fluid dynamics (CFD) method can provide flow field information at a much lower cost. The advancement of computer hardware makes numerical simulation of heat exchanger possible. Prithiviraj and Andrews (1998a,b)

* Corresponding author. Tel.: +86 29 8266 5930; fax: +86 29 8266 9106.
E-mail address: yalinghe@mail.xjtu.edu.cn (Y.-L. He).

0009-2509/$ - see front matter © 2008 Elsevier Ltd. All rights reserved.
doi:10.1016/j.ces.2008.05.044

simulated fluid flow and heat transfer of shell-and-heat exchangers with the distributed resistance method combined with volumetric porosities and surface permeability, in which single computational cell included multiple tubes. He et al. (2005) conducted a numerical investigation of three different heat exchangers based on a distributed resistance concept along with a porous medium model. The model and developed codes were used to simulate three kinds of shell-and-tube heat exchangers (vertical baffles, helical baffles, and finned tube banks).

This paper studies the performance of a heat exchanger with single-helical baffles with both experimental and numerical methods. The optimization of the helical baffles is carried out with a CFD tool to improve the characteristics of heat transfer and pressure drop on the shell side of the heat exchanger. The comparisons of the performance of three heat exchangers with different baffles (single-segmental baffles, single-helical baffles, and two-layer helical baffle) are presented based on numerical results. In the following, the numerical approach to deal with such complicated configuration will be presented first, followed by the experimental setup and data processing method. The experimental and numerical results are then reported in parallel to facilitate the comparison between two methods. Finally, the performance of those three heat exchangers are obtained with CFD modeling.

2. Mathematical modeling

2.1. Computational domain

In the present study, the heat transfer and pressure drop performance of heat exchangers with three different baffle configurations were studied numerically. The three configurations are: (a) single-segmental baffles; (b) single-helical baffles; and (c) two-layer helical baffles.

Since the configuration of shell-and-tube heat exchangers is more complicated, and the size of it is usually bigger, it is difficult to acquire a reliable numerical result adopting whole heat exchanger model with a personal computer. According to the periodic geometric characteristic of shell-and-tube heat exchangers, the simulations are conducted for one period of the three heat exchangers by using periodic boundaries in this paper. Configurations of the three heat exchangers with different baffles are illustrated in Fig. 1. In this research, the single-segmental baffles are perpendicular to the tubes with a baffle cut of 25%, and the helical baffles are quadrant-ellipse shaped baffles at an angle of 20° to the tube axis. Because the primary objective of this research is to study the influence of different configurations of shell-side baffles, the tube bundles arrangement in the shell side is identical for all the three heat exchangers. Fig. 2 shows the tube bundles arrangement in the shell side. Detailed physical dimensions of the three heat exchangers are summarized in Table 1. Oil is the working fluid in the shell side and thermophysical properties of the fluid are listed in Table 2.

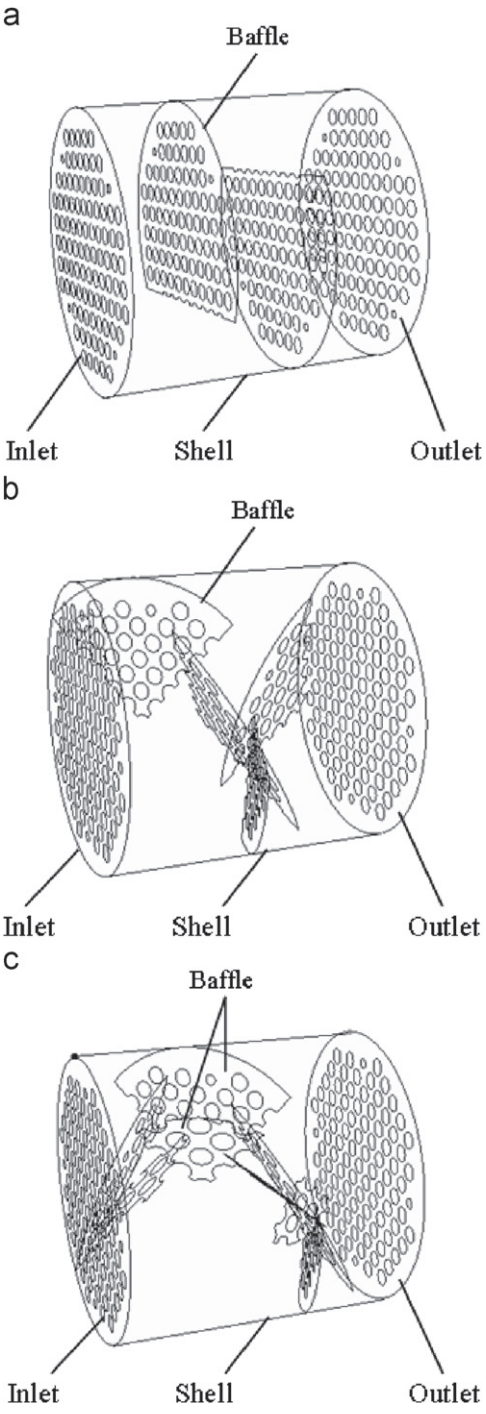

Fig. 1. Configurations of three heat exchangers with different baffles: (a) heat exchanger with single-segmental baffles; (b) heat exchanger with single-helical baffles; (c) heat exchanger with two-layer helical baffles.

2.2. Governing equations and boundary conditions

The renormalization group (RNG) k–ε model of Yakhot and Orszag (1986) is adopted in this study because this model provides improved predictions of near-wall flows and flows with high streamline curvature. The RNG k–ε model was derived by using a statistical technique called renormalization method. Compared with many other sophisticated models (Reynolds stress model and large–eddy simulation model), this model takes shorter computing time and less memory during the simulation process. The RNG k–ε model is widely used in the area of industrial flows and heat transfer because of its economy and accuracy. Therefore, The RNG k–ε turbulence model is adopted for the numerical simulation of the three heat exchangers.

The governing equations for continuity, momentum, energy, k and ε in the computational domain can be expressed as follows:

Continuity:

$$\frac{\partial}{\partial x_i}(\rho u_i) = 0 \tag{1}$$

Momentum:

$$\frac{\partial}{\partial x_i}(\rho u_i u_k) = \frac{\partial}{\partial x_i}\left(\mu \frac{\partial u_k}{\partial x_i}\right) - \frac{\partial p}{\partial x_k} \tag{2}$$

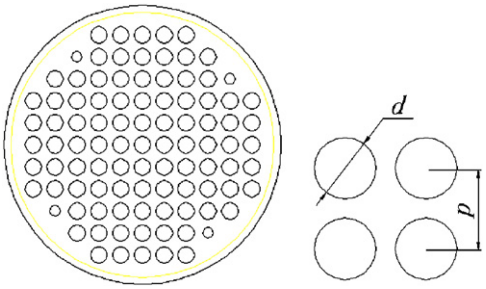

Fig. 2. Tube bundles arrangement in the shell side.

Table 1
Geometric parameters

Dimension	Value
Shell inside diameter (mm)	313
Tube outside diameter (mm)	19
Tube pitch (mm)	25
No. of tubes	93
Length of heat exchanger (mm)	1194
Tube-and-baffle clearance (mm)	0.3
Shell-and-baffle clearance (mm)	1

Table 2
Thermophysical properties of oil

Parameter	Value
C_p (J/kg K)	2270.878
Pr	160
μ(N s/m^2)	0.0094699
ρ(kg/m^3)	826.0872
λ(W/m K)	0.132

Energy:

$$\frac{\partial}{\partial x_i}(\rho u_i T) = \frac{\partial}{\partial x_i}\left(\frac{k}{C_P}\frac{\partial T}{\partial x_i}\right) \tag{3}$$

Turbulent kinetic energy:

$$\frac{\partial}{\partial t}(\rho k) + \frac{\partial}{\partial x_i}(\rho k u_i) = \frac{\partial}{\partial x_j}\left(\alpha_k \mu_{\text{eff}}\frac{\partial k}{\partial x_j}\right) + G_k + \rho\varepsilon \tag{4}$$

Turbulent dissipation energy:

$$\frac{\partial}{\partial t}(\rho\varepsilon) + \frac{\partial}{\partial x_i}(\rho\varepsilon u_i) = \frac{\partial}{\partial x_j}\left(\alpha_\varepsilon \mu_{\text{eff}}\frac{\partial \varepsilon}{\partial x_j}\right) + C_{1\varepsilon}^{*}\frac{\varepsilon}{k}G_k - C_{2\varepsilon}\rho\frac{\varepsilon^2}{k} \tag{5}$$

where

$$\mu_{\text{eff}} = \mu + \mu_t, \quad \mu_t = \rho c_\mu \frac{k^2}{\varepsilon}, \quad C_{1\varepsilon}^{*} = C_{1\varepsilon} - \frac{\eta(1-\eta/\eta_o)}{1+\beta\eta^3},$$

$$\eta = (2E_{ij}\cdot E_{ij})^{1/2}\frac{k}{\varepsilon}, \quad E_{ij} = \frac{1}{2}\left[\frac{\partial u_i}{\partial x_j} + \frac{\partial u_j}{\partial x_i}\right].$$

The empirical constants for the RNG k–ε model are assigned the following values:

$$C_\mu = 0.0845, \quad C_{1\varepsilon} = 1.42, \quad C_{2\varepsilon} = 1.68, \quad \beta = 0.012, \quad \eta_o = 4.38.$$

For the periodic fully developed fluid flow, periodic flow has the following characteristics which are periodic boundary conditions:

$$u(x,y,z) = u(x,y,z+s) \tag{6}$$

$$v(x,y,z) = v(x,y,z+s) \tag{7}$$

$$w(x,y,z) = w(x,y,z+s) \tag{8}$$

$$P(x,y,z) - P(x,y,z+s) = P(x,y,z+s) - P(x,y,z+2s) \tag{9}$$

Non-slip boundary condition is applied on the wall of the three heat exchangers. The mean velocity is at maximum far away from the wall and sharply decreases in the near-wall region. High magnitude of velocity fluctuation is found adjacent to the wall where the large mean velocity gradients ensure massive turbulence production. To accurately simulate the flow in the near-wall region, the standard wall function method is used for the numerical computation. The first near-wall numerical grid point, P, is located sufficiently far from the wall with the local turbulent Reynolds number much greater than unity. In the region between the wall and node P, the expression for velocity can be written as:

$$\frac{u}{u^*} = \begin{cases} y^+, & y^+ \leqslant 11.225 \\ \dfrac{1}{\kappa}\ln(Ey^+), & y^+ > 11.225 \end{cases} \tag{10}$$

where u is the velocity component in flow direction; y is the normal distance from the wall; y^+ is the dimensionless y ($y^+ = \rho y u^*/\mu$); κ is the von Kármán constant ($\kappa = 0.41$); E is the empirical constant ($E = 9.81$); outside of the viscous sub-layer, the friction velocity defined as $\sqrt{\tau_w/\rho}$, is computed as $u^* = C_\mu^{1/4}k^{1/2}$.

In the near-wall cell, the value of the dissipation rate of the turbulent kinetic energy is defined as

$$\varepsilon = \frac{C_\mu^{3/4}k^{3/2}}{ky} \tag{11}$$

The wall heat flux is computed as

$$q_w = \rho C_\rho u^* \Delta T/T^+ \tag{12}$$

where T^+ is estimated by

$$T^+ = \begin{cases} Pr\dfrac{u}{u^*}, & y^+ \leqslant 11.225 \\ Pr_w\left(\dfrac{u}{u^*} + P_T\right), & y^+ > 11.225 \end{cases} \tag{13}$$

$$P_T = \frac{\pi/4}{\sin(\pi/4)}\left(\frac{A_T}{k}\right)^{1/2}\left(\frac{Pr}{Pr_w} - 1\right)\left(\frac{Pr_w}{Pr}\right)^{1/4} \tag{14}$$

where Pr is the molecular Prandtl number; Pr_w is the turbulent wall Prandtl number ($Pr_w = 1.2$); and A_T is the Van Driest constant ($A_T = 26$).

2.3. Solution procedure

The computational domain is meshed with unstructured Tet/Hybrid grids, which are generated by the commercial code GAMBIT due to its excellent merit of managing very complex 3D geometries. The region adjacent to the tube is meshed much finer with the help of successive ratio scheme in GAMBIT. Before any computational result can be deemed enough to illuminate the physical phenomenon, it must be justified through a grid independence test. In the present computation, a series of grid independence tests have been conducted to ensure that optimized computational mesh was obtained. Grid independence tests have been carried out for each mesh model. The grid is refined according to heat transfer coefficients, which results in increase in number of elements by 2–3 times. The following mesh modes having approximately 2 217 000 elements, 2 880 000 elements, 2 980 000 elements, respectively, are adequate for the three configurations (single-segmental baffles, single-helical baffles, and two-layer helical baffles).

The computer code FLUENT is used to calculate the fluid flow and heat transfer in the computational domain. The governing equations are iteratively solved by the finite-volume-method with SIMPLE

pressure–velocity coupling algorithm. For the solution algorithm, the segregated approach is selected. This means that the segregated approach is used to solve a single variable field by considering all cells at the same time, and then solves the next variable field by again considering all cells at the same time. The convective terms in governing equations are discretized by QUICK scheme with three-order precision. Because of the nonlinearity of the equation set being solved by FLUENT, the iterative technique with under-relax predictions of velocity and pressure is used. Default under-relaxation factors of the solver are employed, which are 0.3, 0.7, 0.8, and 0.8 for the pressure, momentum, turbulent kinetic energy, and turbulent energy dissipation, respectively. The convergence criterion is that the normalized residuals are less than 10^{-5} for the flow equations and 10^{-8} for the energy equation. The present computations are performed with a personal computer with CPU frequency of 4 GHz, and usually took approximately 28 h for each task.

3. Experimental study

In the present study, the pressure drop and heat transfer of heat exchangers with single-segmental and single-helical baffles were studied experimentally. The baffles of the heat exchanger with single-segmental baffles are perpendicular to the tubes with a baffle cut of 25% and baffle spacing of 130 mm, and eight segmental baffles are positioned in the shell side of the heat exchanger. The baffle of the heat exchanger with single-helical baffles are quadrant-ellipse shaped baffle at an angle of 20° to the tube axis which occupies one quadrant of the cross section of the shell, and six periods are included in the shell side of the heat exchanger.

3.1. Experimental setup and operating procedure

The experimental setup of the study is shown in Fig. 3. The system includes two independent loops: a cooling water loop (the upper loop in Fig. 3) and a heating oil loop (the lower loop in Fig. 3). The heating oil loop consists of an oil pump, a volumetric flow meter, a heater, and a heat exchanger. The oil is heated up by a heater to reach a predetermined inlet temperature value before entering the shell side of the heat exchanger. Then it is pumped to the shell side, where it is cooled down. Finally, the cooled oil returns to the heater. The cooling water loop consists of a water pump, a volumetric flow meter, a heat exchanger, and a cooling tower. The cooling water is pumped to the tube side of the heat exchanger for heat-up. Then it is cooled down in a cooling tower before returning to the system. A dedicated valve is used to control the cooling water's volumetric flow rate. In order to maintain a stable flow for the cooling water, a tank is designed for the system. To minimize heat loss of the facility, fiberglass insulation at 40 mm thickness is covered on the outer surface of the heat exchanger.

Measurements of inlet and outlet fluid temperatures are carried out using Pt100 sensor. The volumetric flow is measured with a flow meter at a range of 0–60 m^3/h and the signal is transmitted to an electrical transmitter, which provides an electrical output in the range of 4–20 mA. The pressure difference between inlet and outlet of the shell side is measured with a differential pressure transmitter with precision of 0.25% at a range from 0 to 30 kPa. Data Acquisition System (KEITHLEY2700) records readings of the temperature sensor, flow meter and pressure transducer.

The experiment was being conducted under steady state conditions with water and oil as the working fluid. The procedure was

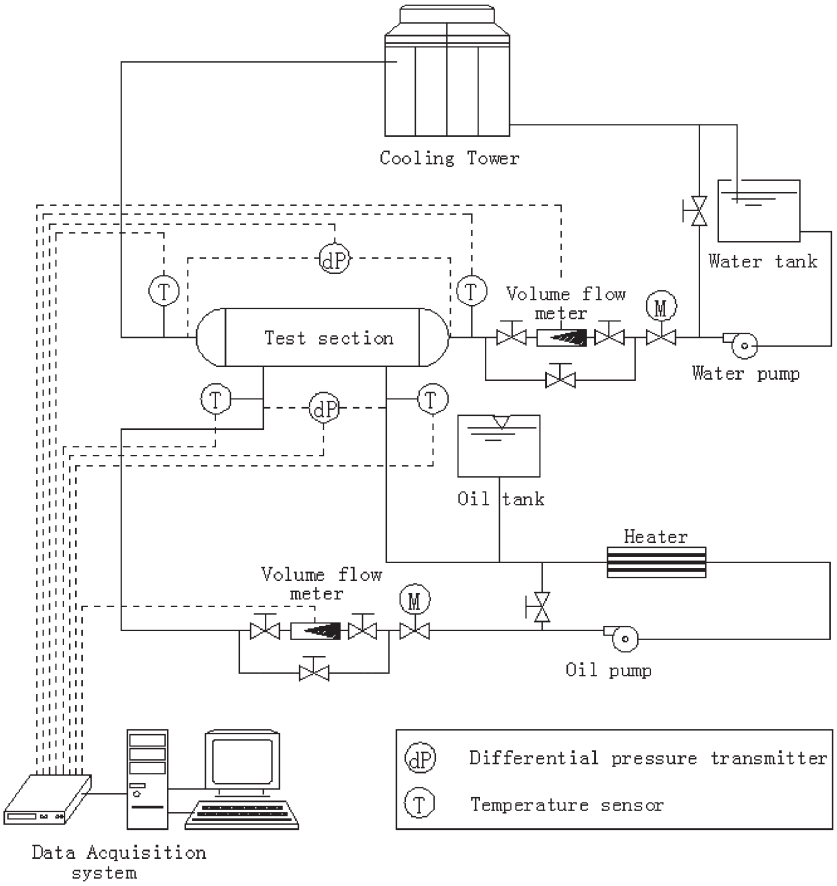

Fig. 3. The experiment setup.

repeated a few times for different flow rates of the shell side ranging from 4 to 24 m^3/h, while the flow rate of the tube was maintained constant. Prior to each experiment, an energy balance test was conducted. Usually, it took approximately 120 min to reach a steady state which was judged by the temperature reading fluctuation of within $\pm 0.1\,^{\circ}C$. After reaching the stable condition, the temperature measured by each Pt100 temperature sensor was recorded by a Data Acquisition System for 10 min maintaining a span of 5 s between two successive readings. At the same time, the volumetric flow rate and the pressure data were recorded.

3.2. Data reduction

The shell-side Reynolds number and friction factor are defined by Eqs. (15) and (16):

$$Re_s = \frac{\rho u_c d_e}{\mu} \tag{15}$$

$$f = \frac{\Delta P}{1/2\rho u_c^2} \cdot \frac{d_e}{L} \tag{16}$$

$$u_c = \frac{q_m}{\rho A_{\min}} \tag{17}$$

where u_c is the mean velocity at the minimum transverse area; d_e is the characteristic dimension which takes the value of the tube diameter d; q_m is the shell-side mass flow rate; ρ is the fluid density; L is the length of the tube; and $A_{\min}$ is the minimum transverse area, which is determined by

$$A_{\min} = \frac{1}{2}BD\left(1 - \frac{d}{p}\right) \tag{18}$$

where B is the axial distance of a period; D is the diameter of shell side; and p is the tube pitch.

Prior to experimental run, a heat balance test was conducted. The difference of heat duties between the hot oil and cooling water needs to be within 5.0% for all runs. The heat balance equation is

$$\left|\frac{Q_s - Q_t}{Q_{\text{ave}}}\right| \leqslant 5.0\% \tag{19}$$

$$Q_{\text{ave}} = \frac{Q_s + Q_t}{2} \tag{20}$$

$$Q_s = \rho_s \times V_s \times C_{p,s}(T_{s,\text{in}} - T_{s,\text{out}}) \tag{21}$$

$$Q_t = \rho_t \times V_t \times C_{p,t}(T_{t,\text{out}} - T_{t,\text{in}}) \tag{22}$$

where Q_s and Q_t are heat transfer rate of the shell side and the tube side; $T_{s,\text{in}}$ and $T_{s,\text{out}}$ are shell-side temperature at the inlet and outlet, respectively; $T_{t,\text{in}}$ and $T_{t,\text{out}}$ are tube-side temperature at the inlet and outlet. $C_{p,s}$ and $C_{p,t}$ are specific heat of oil and water. The thermodynamic and transport properties of water and oil are calculated according to average temperature values of the inlet and outlet for the section.

The overall heat transfer coefficient, U, is equal to

$$U = \frac{Q_{\text{ave}}}{A\,\Delta T_{LMTD}} \tag{23}$$

where A is the surface area, and ΔT_{LMTD} is the log mean temperature difference, which is determined by

$$\Delta T_{LMTD} = \frac{\Delta T_2 - \Delta T_1}{\ln(\Delta T_2/\Delta T_1)} \tag{24}$$

$$\Delta T_1 = T_{s,\text{out}} - T_{t,\text{in}}, \quad \Delta T_2 = T_{s,\text{in}} - T_{t,\text{out}} \tag{25}$$

Heat transfer coefficients of the shell side are calculated with traditional Wilson plots technique as described by Rose (2004). Wilson plots technique is applied by calculating overall heat transfer coefficients for a number of trails where fluid flow of one side is kept constant and fluid of the other side is varied. In this study, the flow inside the tubes is kept constant and the flow of the shell side varies. It is assumed that the tube-side heat transfer coefficient is constant at a constant volumetric flow rate. The tube-side heat transfer coefficient is calculated with Gnielinski (1976) Equation

$$Nu_t = \frac{(f_t/8)(Re_t - 1000)Pr_t}{1 + 12.7\sqrt{f_t/8}(Pr_t^{2/3} - 1)}\left[1 + \left(\frac{d}{L}\right)^{2/3}\right]c_t \tag{26}$$

$$c_t = \left(\frac{Pr_t}{Pr_w}\right)^{0.11} \tag{27}$$

$$f_t = (1.82 lg\, Re_t - 1.64)^{-2} \tag{28}$$

Once the Nusselt numbers are determined, the tube-side heat transfer coefficient is obtained from the conventional definition

$$h_t = \lambda_t \frac{Nu_t}{d} \tag{29}$$

The overall heat transfer coefficient is given by the relation

$$\frac{1}{U} = \frac{1}{h_s} + \frac{A_s}{A_t}R_w + \frac{A_s}{A_t h_t} \tag{30}$$

In this equation, A_t and A_s are inside and outside surface area of tube, respectively, R_w is the thermal resistance of the tube wall, which is defined as

$$R_w = \frac{d_{\text{inner}} \ln(d_{\text{outer}}/d_{\text{inner}})}{2\lambda} \tag{31}$$

Substituting Eq. (29) into Eq. (30) after calculating the overall heat transfer coefficients, the shell-side heat transfer coefficients are calculated. Then, the shell-side Nusselt numbers is computed by the following equation:

$$Nu_s = \frac{h_s d}{\lambda_s} \tag{32}$$

3.3. Experimental uncertainty

The experimental uncertainty of the present work is determined by using the method presented by Kline and McClintock (1953). The uncertainty calculation method involves calculating derivatives of the desired variable with respect to individual experimental quantities and applying known uncertainties. According to the reference, the experimental uncertainty is defined as follows:

$$W_R = \sqrt{\left(\frac{\partial R}{\partial x_1}W_{x_1}\right)^2 + \left(\frac{\partial R}{\partial x_2}W_{x_2}\right)^2 + \cdots\cdots + \left(\frac{\partial R}{\partial x_n}W_{x_n}\right)^2} \tag{33}$$

where $R = f(x_1, x_2, \ldots, x_n)$ and x_n is the variable that affects the results of R.

For heat exchanger with single-segmental baffles, the uncertainties involved in the friction factors and Nusselt number are within $\pm 5.5\%$ and $\pm 12.1\%$, respectively. For heat exchanger with single-helical baffles, the uncertainties involved in the friction factors and Nusselt number are within $\pm 4.6\%$ and $\pm 8.2\%$, respectively.

4. Results and discussion

In the present study, experimental studies are conducted for the single-segmental baffles and single-helical baffles heat exchangers and the optimization of the helical baffles is carried out with a CFD tool. Finally, the comparisons of the performance of the three heat

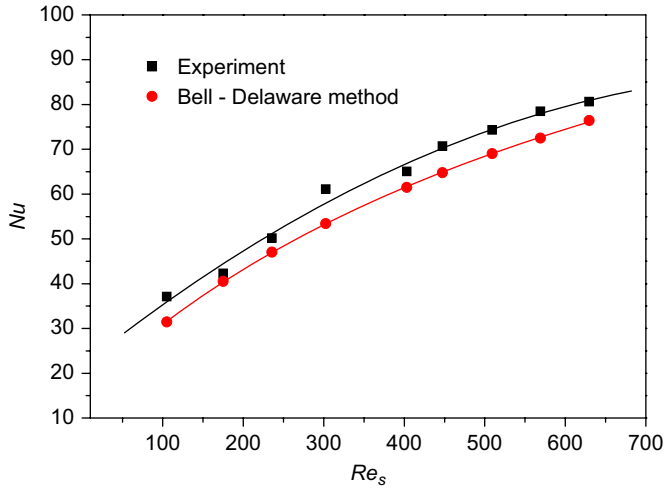

Fig. 4. Comparison of experimental results of Nusselt number with the data from Bell–Delaware method (Bell, 1981) for single-segmental heat exchanger.

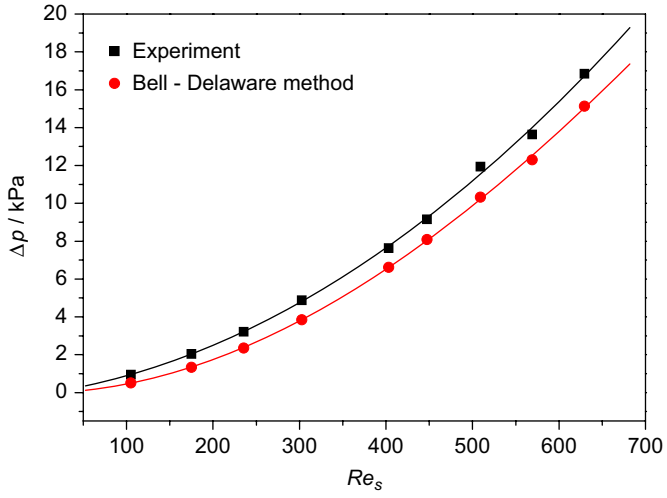

Fig. 5. Comparison of experimental results of pressure drop with the data from Bell–Delaware method (Bell, 1981) for single-segmental heat exchanger.

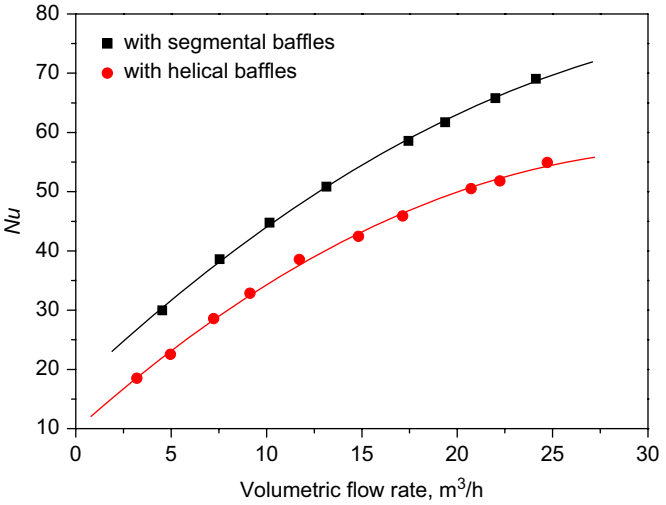

Fig. 6. Nusselt number versus volumetric flow rate for heat exchangers with single-segmental baffles and single-helical baffles (experimental).

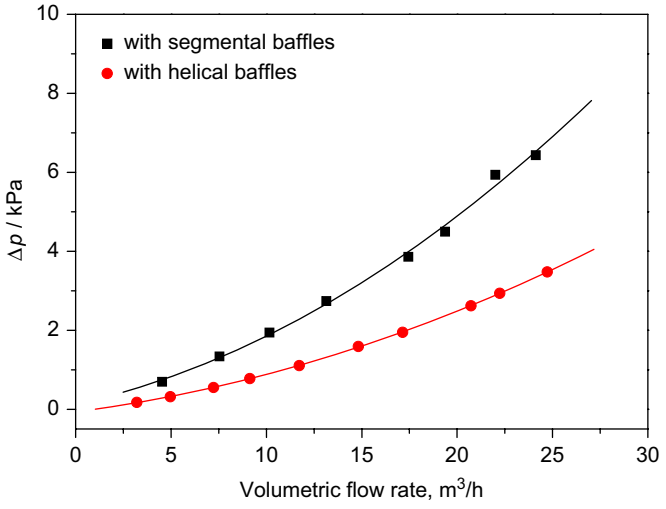

Fig. 7. Pressure drop versus volumetric flow rate for heat exchangers with single-segmental baffles and single-helical baffles (experimental).

exchangers with different baffles (single-segmental baffles, single-helical baffles, and two-layer helical baffle) are presented based on numerical results. The details of the data source in the paper are illustrated in Table 3.

4.1. Experimental results

In order to verify the experimental set-up, a heat exchanger with single-segmental baffles is used to investigate heat transfer and pressure drop at the early stage of the experiment. The heat transfer measurements of the present work are compared with the data from Bell–Delaware method (Bell, 1981, 1988). Fig. 4 shows the comparison of experimental results of Nusselt number with the data from Bell–Delaware method for the single-segmental heat exchanger. It is seen from the figure that the Nusselt numbers in the present work are consistently higher than the results from the Bell–Delaware method. The difference between the present experimental data and the results from the Bell–Delaware method is approximately 10%. The comparison of experimental results of pressure drop with the data from Bell–Delaware method for the single-segmental heat exchanger is presented in Fig. 5. It can be seen from the figure that the deviation between the present experimental measurements and the results from the literature is about 12%. The present experimental results are in agreement with the data from Bell–Delaware method. It shows that the experiment setup is reliable for the experimental research of shell-and-tube heat exchangers.

Fig. 6 illustrates the Nusselt number versus volumetric flow rate for heat exchangers with single-segmental baffles and single-helical baffles. It can be clearly observed that the heat transfer coefficient of the heat exchanger with single-helical baffles is about 75% the value of the heat exchanger with single-segmental baffles. The Nusselt numbers of the heat exchanger with single-helical baffles can be expressed as a function of the shell-side Reynolds number.

$$Nu_s = 0.275 Re_s^{0.55} Pr_s^{1/3} \quad (50 < Re_s < 1000) \tag{34}$$

Fig. 7 shows the pressure drop versus volumetric flow rate for heat exchangers with single-segmental baffles and single-helical baffles. It is clear that the pressure drop of the heat exchanger with single-helical baffles is lower than that of the heat exchanger with single-segmental baffles at the same volumetric flow rate. The pressure

Table 3
Data source of the text

Heat exchanger type	Numerical results	Experimental results
Single-segmental baffles	Present research	Present research and results from Bell–Delaware method (Bell, 1981)
Single-helical baffles	Present research	Present research
Two-layer helical baffles	Present research	–

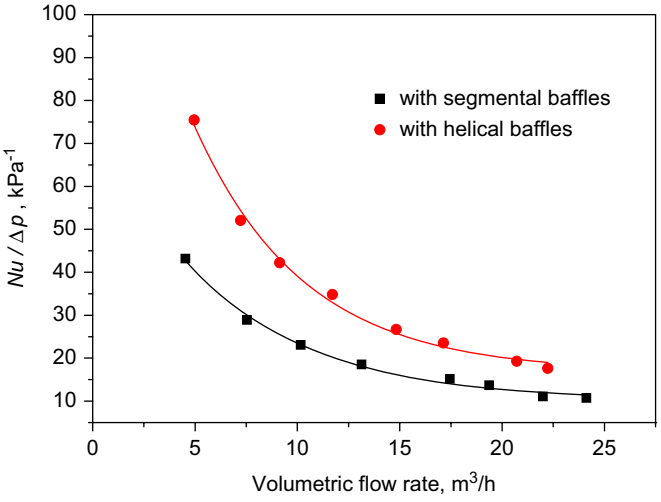

Fig. 8. Ratio of heat transfer to pressure drop for heat exchangers with single-segmental baffles and single-helical baffles (experimental).

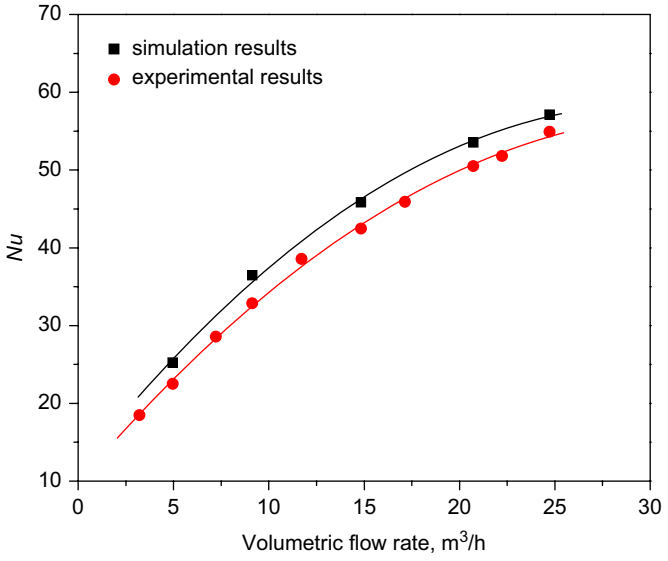

Fig. 9. Comparison of experimental results of Nusselt number with the numerical data for single-helical heat exchanger.

drop of the heat exchanger with single-helical baffles is only approximately 45–55% of that of the heat exchanger with single-segmental baffles. It can be explained as: for a single-segmental heat exchanger, the flow pattern on the shell side is zigzag, and flow separation at the edge of baffles causes abrupt momentum change and severe pressure loss; whereas the primary flow direction of the heat exchanger with single-helical baffles does not change dramatically. The friction factor for the heat exchanger with single-helical baffles can be expressed as a function of the shell-side Reynolds number:

$$f_s = 20.06(Re_s)^{-0.56} (Re_s < 400) \quad (35)$$

$$f_s = 11.34(Re_s)^{-0.47} (400 < Re_s < 1000) \quad (36)$$

Proper evaluation is important for comparing the integrated performance of different heat exchangers. Both heat transfer coefficient and pressure drop are important parameters for heat exchangers. It is desirable to obtain the highest heat transfer rate at the lowest pressure drop, so the ratio of heat transfer coefficient to pressure drop is used as a comparison criterion in the present study. The ratio of heat transfer to pressure drop for heat exchangers with single-segmental baffles and single-helical baffles is shown in Fig. 8. The effectiveness of the heat exchanger with single-helical baffles is obviously higher than that of the heat exchanger with single-segmental baffles. In the figure, about 35–65% enhancement in the ratio of heat transfer coefficient to the same pressure drop for the heat exchanger with single-helical baffles is observed. It means that the pumping cost for a heat exchanger with single-helical baffles is much less than that of the heat exchanger with single-segmental baffles at a given heat duty. It was mentioned earlier that, in comparison between the heat exchangers with single-segmental baffles and single-helical baffles, decrease in pressure drop is larger than decrease in heat transfer coefficient. This is the reason why the heat exchanger with single-helical baffles has a higher effectiveness of heat transfer to pressure drop than that of the heat exchanger with single-segmental baffles.

4.2. Model validation

For an investigation at a wide range of geometries, experimental study would be costly and time-consuming. CFD simulations avoid the difficulty and cost in establishing an experimental facility, and are capable of carrying out in-depth study on the flow field that is difficult to simulate by an experimental way.

Fig. 9 depicts the comparison of experimental results of Nusselt number with the numerical data for single-helical heat exchanger. It can be observed that the two sets of data have a good agreement in trend and the pressure drop by numerical prediction is approximately 8% higher than the experimental results for all volumetric flow rates. The comparison of experimental results of pressure drop with the numerical data for single-helical heat exchanger is shown in Fig. 10. It indicates that the error between CFD prediction and experimental result is about 10% for the heat exchanger with single-helical baffles. CFD tends to overpredict the pressure drop at higher volumetric flow rate. Because of manufacturing tolerances and quality control, the baffles might have leakage streams during the experiment, so the effective mass flow rate across the tube bundle decreases resulting in decrease in the experimental shell-side heat transfer coefficient. However, the effects of the leakage streams are not taken into account in numerical prediction. Because the discrepancy is small, the numerically predicted results can be acceptable in engineering application.

4.3. Comparison of different shell-and-tube heat exchangers

In the present study, the heat transfer and pressure drop performance of heat exchangers with three different baffle configurations were studied numerically. The three configurations are

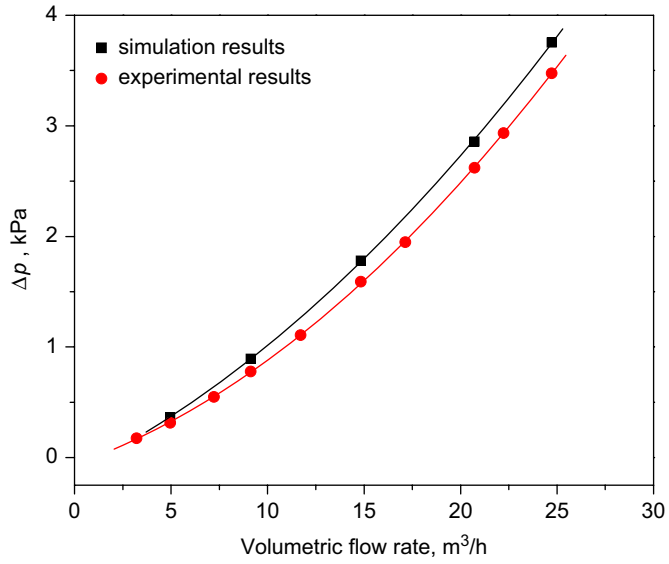

Fig. 10. Comparison of experimental results of pressure drop with the numerical data for single-helical heat exchanger.

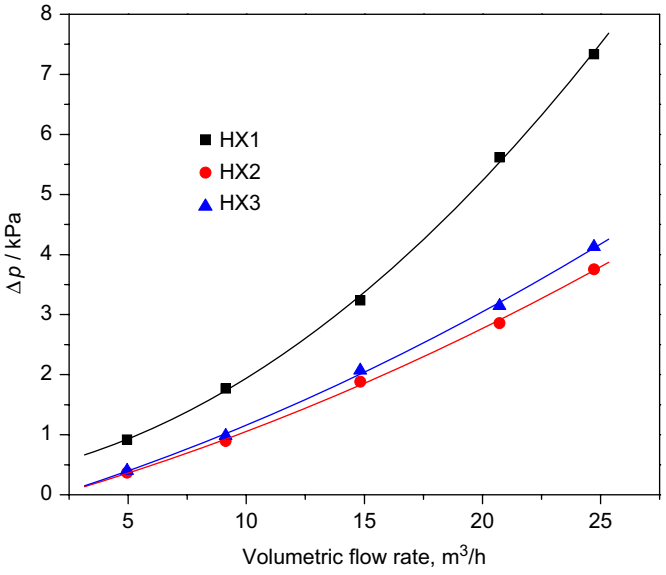

Fig. 12. Pressure drop versus volumetric flow rate for three heat exchangers (simulation).

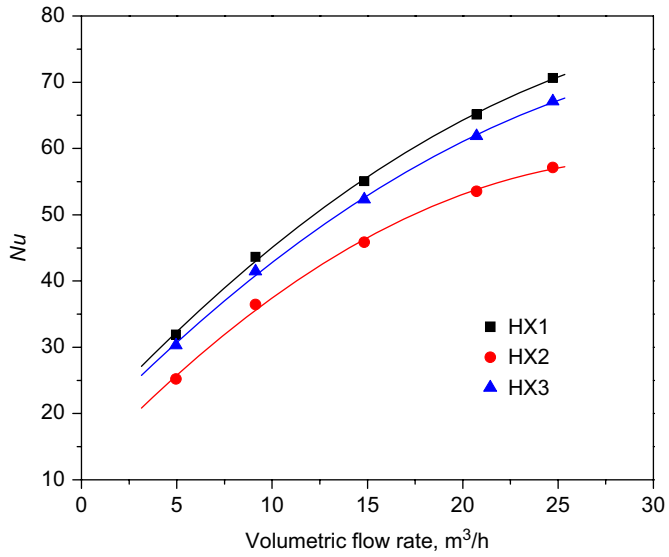

Fig. 11. Nusselt number versus volumetric flow rate for three heat exchangers (simulation).

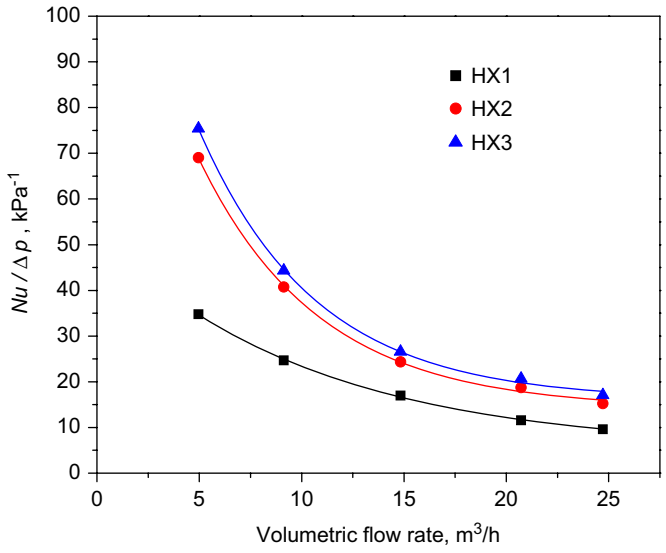

Fig. 13. Ratio of heat transfer to pressure drop for three heat exchangers (simulation).

(a) single-segmental baffles; (b) single-helical baffles; and (c) two-layer helical baffles. For the convenience of discussion, hereinafter, HX1 refers to the heat exchanger with single-segmental baffles, HX2 refers to the heat exchanger with single-helical baffles, and HX3 refers the heat exchanger with two-layer helical baffles.

Fig. 11 shows the Nusselt number versus volumetric flow rate for the three heat exchangers. It can be seen that the Nusselt number increases with the increase of the volumetric flow rate for all three heat exchangers. It can also be seen from Fig. 11 that the Nusselt number of both HX2 and HX3 are lower than that of HX1 at the same volumetric flow rate. The pressure drop versus volumetric flow rate for the three heat exchangers is presented in Fig. 12. It shows that the pressure drop increases with the increase in the volumetric flow rate for all three heat exchangers. It is clear that the pressure drops of both HX2 and HX3 are lower than that of HX1 at the same volumetric flow rate. The pressure drop of HX3 is slightly higher than that of HX2. The reason for this phenomenon appears to be as follows, for single-segmental heat exchanger, the flow pattern on the shell side is zigzag, flow separation at the edge of baffles causes abrupt momentum change and severe pressure loss. Whereas the primary flows direction of the heat exchanger with helical baffles does not change dramatically. Since the inner-baffles of HX3 widen the flow separation along the side edge of the baffles, the pressure drop in HX3 is higher than that of HX2.

In order to compare the effectiveness of heat transfer to pressure drop for different baffles, the ratio of the integral shell-side heat transfer to pressure drop for those three heat exchangers are presented. Fig. 13 shows the comparison of the ratio of heat transfer to pressure drop for the three heat exchangers. The effectiveness of the heat exchanger with helical baffles is obviously higher than that with single-segmental baffles. This means that the overall performance of

heat exchangers with helical baffles is superior to that of the heat exchanger with single-segmental baffles. It can also be seen from Fig. 13 that the ratios of heat transfer coefficient to pressure drop of HX3 is higher (10%) than that of HX2. This is because the optimal baffles (two-layer baffles) not only decrease the stream passing through the gap between neighboring sector plates, but also enhance the turbulence of the shell side, especially in the central region.

5. Conclusions

Numerical and experimental investigations of a heat exchanger with single-helical baffles are performed in the present work. Oil flow is in the shell side while water acts as a coolant flowing inside the tubes. The heat transfer coefficients and pressure drop on the shell side of heat exchangers with helical baffles and segmental baffles based on the experimental study are reported. It shows that the heat transfer coefficient increases with increasing volume flow rate on the shell side for a constant volume flow rate in the tube side. It is found that the heat exchanger with single-helical baffles has 75% of the heat transfer capacity but only about 50% of the pressure drop of the heat exchanger with single-segmental baffles. It further demonstrates that the ratio of heat transfer coefficient to pressure drop of the heat exchanger with single-helical baffles is obviously higher than that of the heat exchanger with single-segmental baffles. It means that the heat exchanger with single-helical baffles has a higher heat transfer rate with the same pumping power consumption.

CFD predicted results for hydrodynamics and heat transfer are in agreement with experimental results. It is concluded that CFD predictions for a new geometric and process configuration can be safely relied upon for design and optimization purpose. The performances of those three shell-and-tube heat exchangers are simulated and analyzed. The heat exchangers with helical baffles have higher heat transfer to the same pressure drop than that of the heat exchanger with segmental baffles based on the present numerical results. The effectiveness of the heat exchanger with two-layer helical baffles is obviously higher (10%) than that of the heat exchanger with single-helical baffles.

Notation

A	heat transfer area, m^2
A_{min}	minimum transverse area, m^2
A_T	Van Driest constant
C_p	specific heat, J/(kg K)
d	tube diameter, m
d_e	characteristic dimension, m
D	shell diameter, m
E	empirical constant in logarithmic velocity profile
f	friction factor
h	heat transfer coefficient, W/(m^2 K)
k	turbulent kinetic energy
L	length of the tube, m
Nu	Nusselt number
p	tube pitch, m
ΔP	pressure drop, Pa
Pr	Prandtl number
Pr_w	turbulent wall Prandtl number
q_m	shell-side mass flow rate, kg/s
Q	heat transfer rate, J/s
R_w	thermal resistance of the tube wall
Re	Reynolds number
T	temperature, K
ΔT_{LMTD}	log-mean temperature difference, K
u	velocity, m/s
u_c	mean velocity at the minimum transverse area, m/s
u^*	frictional velocity ($u^* = \sqrt{\tau_w/\rho}$), m/s
U	overall heat transfer coefficient, W/(m^2 K)
V	volumetric flow rate, m^3/s
y	normal distance from the wall
y^+	dimensionless y

Greek letters

ε	turbulent energy dissipation
κ	Von Kármán constant
λ	thermal conductivity, W/(m K)
μ	dynamic viscosity, N s/m^2
ρ	density, kg/m^3
τ_w	wall shear stress, N/m^2

Subscripts

ave	average
in	inlet
out	outlet
s	shell side
t	tube side
w	wall
$+$	standard wall coordinates

Acknowledgments

This work is supported by the Key Project of National Natural Science Foundation of China (No. 50736005), the National Basic Research Program of China (973 Program) (2007CB206902) and the Key grant Project of Chinese Ministry of Education (No. 306014).

References

Bell, K.J., 1981. Delaware method for shell side design. In: Kakac, S., Bergles, A.E., Mayinger, F. (Eds.), Heat Exchangers-Thermal-Hydraulic Fundamentals and Design. Taylor & Francis, Washington DC.

Bell, K.J., 1988. Delaware method of shell-side design. In: Shah, R.K., Sunnarao, E.C., Mashelkar, R.A. (Eds.), Heat Transfer Equipment Design. Taylor & Francis, New York.

Bell, K.J., 2004. Heat exchanger design for the process industries. ASME Journal of Heat Transfer 126 (6), 877–885.

Gnielinski, V., 1976. New equations for heat and mass transfer in turbulent pipe and channel flows. International Chemical Engineering 16, 359–368.

He, Y.L., Tao, W.Q., Deng, B., Li, X., Wu, Y., 2005. Numerical simulation and experimental study of flow and heat transfer characteristics of shell side fluid in shell-and-tube heat exchangers. In: Proceedings of Fifth International Conference on Enhanced, Compact and Ultra-Compact Heat Exchangers: Science, Engineering and Technology, Hoboken, NJ, USA, pp. 29–42.

Kline, S.J., McClintock, F.A., 1953. Describing uncertainties in single-sample experiments. Mechanical Engineering 75 (1), 3–8.

Kral, D., Stehlik, P., Van Der Ploeg, H.J., Master, Bashir, I., 1996. Helical baffles in shell-and-tube heat exchangers, part I: experimental verification. Heat Transfer Engineering 17 (1), 93–101.

Li, H.D., Kottke, V., 1998. Effect of baffle spacing on pressure drop and local heat transfer in shell-and-tube heat exchangers for staggered tube arrangement. International Journal of Heat and Mass Transfer 41 (10), 1303–1311.

Lutcha, J., Nemcansky, J., 1990. Performance improvement of tubular heat exchangers by helical baffles. Trans. I.Ch.E. 68 (A), 263–270.

Mukherjee, R., 1992. Use double-segmental baffles in the shell-and-tube heat exchangers. Chemical Engineering Progress 88, 47–52.

Prithiviraj, M., Andrews, M.J., 1998a. Three-dimensional numerical simulation of shell-and-tube heat exchangers, part I: foundation and fluid mechanics. Numerical Heat Transfer, Part A 33, 799–816.

Prithiviraj, M., Andrews, M.J., 1998b. Three-dimensional numerical simulation of shell-and-tube heat exchangers, part II: heat transfer. Numerical Heat Transfer, Part A 33, 817–828.

Rose, J.W., 2004. Heat-transfer coefficient, Wilson plots and accuracy of thermal measurements. Experimental Thermal and Fluid Science 28 (2–3), 77–86.

Saffar-Avval, M., Damangir, E., 1995. A general correlation for determining optimum baffle spacing for all types of shell and tube exchangers. International Journal of Heat and Mass Transfer 38 (13), 2501–2506.

Soltan, B.K., Saffar-Avval, M., Damangir, E., 2004. Minimization of capital and operating costs of shell and tube condensers using optimum baffle spacing. Applied Thermal Engineering 24 (17–18), 2801–2810.

Stehlik, P., Nemcansky, J., Kral, D., Swanson, L.W., 1994. Comparison of correction factors for shell-and-tube heat exchangers with segmental or helical baffles. Heat Transfer Engineering 15 (1), 55–65.
Sthlik, P., Wadekar, V.V., 2002. Different strategies to improve industrial heat exchange. Heat Transfer Engineering 23 (6), 36–48.
Wang, S.L., 2002. Hydrodynamic studies on heat exchangers with helical baffles. Heat Transfer Engineering 23 (3), 43–49.
Webb, R.L., 1994. Principles of Enhanced Heat Transfer. Wiley, New York.
Yakhot, V., Orszag, S.A., 1986. Renormalization group analysis of turbulence, I: basic theory. Journal of Scientific Computing 1, 3–11.
Zhang, Z.G., Xu, T., Fang, X.M., 2004. Experimental study on heat transfer enhancement of a helically baffled heat exchanger combined with three-dimensional finned tubes. Applied Thermal Engineering 24 (14–15), 2293–2300.